Water Air Soil Pollut (2014) 225:1784
DOI 10.1007/s11270-013-1784-x

Effect of Inorganic Salt Mixtures on Phenol Mineralization by Photo-Fenton-Analysis via an Experimental Design

Syllos Santos da Silva · Osvaldo Chiavone-Filho · Eduardo L. de Barros Neto · Edson Luiz Foletto · André Luís N. Mota

Received: 14 June 2013 / Accepted: 16 October 2013 / Published online: 29 November 2013

Abstract Effluents of resin production, petrochemicals, refineries, paper mills, and iron foundry industries may present high concentrations of phenol. The high toxicity, solubility, and stability of phenolic compounds hamper the treatment of this wastewater by conventional methods. In this work, the effect of inorganic ion mixtures, such as chloride, nitrate, sulfate, carbonate, and monophosphate on the phenol mineralization by the photo-Fenton process, was investigated. The kinetic of phenol mineralization was monitored with the analysis of total organic carbon. Two experimental designs were employed to evaluate the influence of inorganic ions on mineralization efficiency: fractional experimental design and central composite rotatable design (CCRD). The pollutant degradation reached 100 % at 60 min in the absence of salts, but in a saline medium, this value was reduced to 10 %. The sequence of the inhibitory effect was $H_2PO_4^- \gg Cl^- > SO_4^{2-} > NO_3^- \approx CO_3^{2}$. The statistical data analysis showed that the phosphate and chloride ion concentrations were studied variables and statistically significant on the mineralization process. The analysis of variance showed: (1) good fit between the observed and prediction values for fractional experiment design and CCRD and (2) according to Fisher distribution, the models that were obtained were considered significant and predictive.

Keywords Inorganic ions · Phenol · Photo-Fenton · Experimental design · Response surface

S. Santos da Silva · O. Chiavone-Filho · E. L. de Barros Neto
Department of Chemical Engineering, NUPEG, Federal University of Rio Grande do Norte,
Natal, RN 59072-970, Brazil

E. L. Foletto (✉)
Department of Chemical Engineering, Federal University of Santa Maria,
Santa Maria, RS 97105-900, Brazil
e-mail: efoletto@gmail.com

A. L. N. Mota
Department of Environmental Science and Technology, Federal University of Rural Semi-Arid,
Mossoró, RN 59625-900, Brazil

1 Introduction

Industrial effluents from refineries, paper mill, petrochemistry, and iron foundry production may present high concentrations of phenol and its derivatives (Kavitha and Palanivelu 2004). In addition, the produced water in an oilfield contains phenol and high amounts of salts. Conventional biological treatment of phenolic effluents is complicated by toxicity, in combination with high solubility and stability of these compounds into an aqueous solution (Huang et al. 2010). Many researchers have proposed different methods to remove or degrade phenol into effluents, such as liquid membrane-based extraction (Reis et al. 2011), adsorption on activated carbon (Rodrigues et al. 2011), modified polymers (Saitoh et al. 2011), photo-Fenton (Navarro et al. 2010), and sono-Fenton and sono–photo-Fenton (Babuponnusami and Muthukumar 2011). Among these methods, the advanced oxidation processes (AOP) stand out as an alternative to degrade recalcitrant compounds in industrial wastewater.

It is a common characteristic among all AOP, wherein the production of hydroxyl radicals is derived from several reaction paths (Gernjak et al. 2003). The photo-Fenton process has been largely applied in organic pollutant degradation (Devi et al. 2010; Masomboon et al. 2010; Silva et al. 2012). On this process, hydroxyl radical generation occurs in two steps (Krutzler and Bauer 1999): Fenton step, which produces hydroxyl radicals from the reaction between ferrous ion and hydrogen peroxide (Eq. 1), and photocatalytic step, which comprises hydrolyzed compounds photolysis with Fe^{3+} (formed on the first step) and generates more hydroxyl radicals and regenerates ferrous ions (Fe^{2+}) (Eqs. 2 and 3). The hydroxyl radicals formed (E=2.8 V) attacks organic material, leading to its oxidation (Eq. 4).

$$Fe^{2+} + H_2O_2 \rightarrow Fe^{3+} + HO^{\bullet} \quad (1)$$

$$[Fe(OH)]^{2+} \xrightarrow{h\nu} Fe^{2+} + HO^{\bullet} \quad (2)$$

$$[Fe(COOCR)]^{2+} \xrightarrow{h\nu} Fe^{2+} + CO_2 + R^{\bullet} \quad (3)$$

$$HO^{\bullet} + RH \rightarrow \text{oxidized products} \rightarrow CO_2 + H_2O \quad (4)$$

A few works have reported the influence of inorganic anions on the mineralization efficiency of organic pollutants by the photo-Fenton process (Moraes et al. 2004; Bacardit et al. 2007; Machulek et al. 2007). Most researchers have evaluated the efficiency of the photo-Fenton process on the organic compound degradation with only one salt at once. However, works reporting the simultaneous presence of several salts are scarce. Therefore, the synergetic effect has been poorly investigated.

In this context, the aim of this work was to evaluate the effect of inorganic salts on phenol mineralization by the photo-Fenton process. The mixture was composed of the following sodium salts: sodium chloride (NaCl), sodium nitrate ($NaNO_3$), sodium sulfate ($NaSO_4$), sodium carbonate (Na_2CO_3), and monosodium phosphate (NaH_2PO_4). This study was conducted using the statistic tool of fractional factorial and central composite rotatable design (CCRD).

2 Materials and Methods

2.1 Materials

All of the reagents that were used were of analytical grade and supplied by VETEC: sulfuric acid (H_2SO_4), Na_2CO_3, sodium chloride (NaCl), phenol (C_6H_5OH), NaH_2PO_4, sodium hydroxide (NaOH), potassium iodide (KI), $NaNO_3$, anhydrous sodium sulfite (Na_2SO_3), hydrogen peroxide (H_2O_2) (30 %), sodium sulfate (Na_2SO_4), and ferrous sulfate heptahydrate ($FeSO_4 \cdot 7H_2O$).

2.2 Apparatus and Analytical Procedure

Synthetic effluent was prepared from the dissolution of phenol and sodium salts into distilled water. For each experiment, 4 L of effluent were prepared. Sodium sulfate heptahydrate ($FeSO_4 \cdot 7H_2O$) and H_2O_2 (30 %) were used as Fenton reagents.

Experiments were carried out in a tubular photochemical reactor that consists of four modules and is connected to a mixing tank. At the center of each reactor module, a quartz tube for the effluent circulation was set. Fluorescent lamps (Sylvania, black light, 40 W) were used as a UVA radiation source (320–400 nm) for each reactor module. A centrifuge pump was used for effluent circulation in the system.

Effluent pH was adjusted between 2.5 and 3.0 with an H_2SO_4 dilute solution. Then, ferrous sulfate was added into the reaction medium. H_2O_2 dosages were carried out in system in a predetermined reaction time at 0, 20, and 45 min. Samples were collected at predetermined times (0, 5, 10, 15, 20, 30, 45, 60, and 90 min) and an inhibitor solution was added (NaOH, Na_2SO_3, and KI—0.1 N) in order to interrupt the reaction. Samples were filtered (0.45 μm, Millipore) before the analysis of total organic carbon (TOC, V-CPH/Shimadzu). For all experiments, concentrations of $TOC_{(initial)}$, Fe^{2+}, and H_2O_2 were kept constant in 200 ppm, 1 mM, and 200 mM, respectively.

2.3 Experimental Design

The full factorial design is denoted by N^k, where N is the number of levels of the dependent variable, and k is the number of independent variables (Box et al. 2005). The experimental region is described by Eq. 5, where y_i is the answer in the condition of i; x_i are the coded levels

for the independent variables; β_0, β_i, β_{ii}, and β_{ij} are adjustable model parameters; ε is the random error associated with this measure (Trinh and Kang 2011). The coefficients estimation of the polynomial model was arrived at by the least squares method.

$$y_i = \beta_0 + \sum_{i=1}^{n} \beta_i x_i + \sum_{i=1}^{n} \beta_{ii} x_i^2 + \sum_{i<j}^{n} \beta_{ij} x_i x_j + \varepsilon \quad (5)$$

It is possible, through the execution of a fraction of the full factorial design, to obtain the same information, in most cases, of the most important effects with a lower number of assays (Teófilo and Ferreira 2006). This type of design is known as fractionated factorial, generally represented by 2^{k-b}, where k is the number of variables, and b is the size of the fraction.

A fractional factorial design (2^{5-1}) was applied to identify the independent variables with more influence on the response variable. Concentrations of NaCl, Na_2SO_4, Na_2CO_3, and NaH_2PO_4 were selected as independent variables, and the efficiency of phenol mineralization was selected as a response variable. Table 1 presents codified levels of the variables studied, where (−1) represents the inferior level, (0) the central point, and (+1) as the higher level.

A full factorial design was performed to enlarge the range of anion concentration studied in order to better evaluate the effects of independent variables on the response. A CCRD was applied in order to evaluate the effect of NaCl and Na_2SO_4 concentrations upon the efficiency of phenol mineralization. Table 2 presents the codified values of independent variables. In all cases, the order of the experiments was random in order to avoid any interference with the results.

Table 1 Fractional factorial design 2^{5-1} for the phenol mineralization

Variable	x_i	−1	0	+1
[NaCl] ppm	x_1	100	245	390
[Na_2SO_4] ppm	x_2	100	245	390
[Na_2CO_3] ppm	x_3	100	245	390
[NaH_2PO_4] ppm	x_4	100	245	390
[$NaNO_3$] ppm	x_5	100	245	390

Table 2 Central composite rotatable design (CCRD) for phenol mineralization

Variable	x_i	−1.41	−1	0	+1	+1.41
[NaCl] ppm	x_1	0.04	857.90	2,928.95	5,000	5,857.86
[Na_2SO_4] ppm	x_2	0.04	857.90	2,928.95	5,000	5,857.86

3 Results and Discussion

3.1 Kinetics of Phenol Mineralization

Preliminary experiments were carried out in order to evaluate the effects of NaCl, $NaNO_3$, $NaSO_4$, Na_2CO_3, and NaH_2PO_4 concentrations on mineralization and to establish levels of independent variables in the experimental design. Figure 1 shows the mineralization kinetics for the following conditions: salt-free effluent (Fig. 1a), effluent containing 100 ppm of each salt (Fig. 1b), and effluent containing 500 ppm of each salt (Fig. 1c). The efficiency of phenol mineralization (η) was calculated by the Eq. 6, where TOC_0 and TOC are the initial total organic carbon concentrations and at time t, respectively.

$$\eta(\%) = 100 - \left(\frac{TOC}{TOC_0} \times 100\right) \quad (6)$$

As can be seen in Fig. 1, the increasing of salt concentration reduces the mineralization efficiency. Similar results were observed by other researchers (Bacardit et al. 2007). The mineralization efficiency in

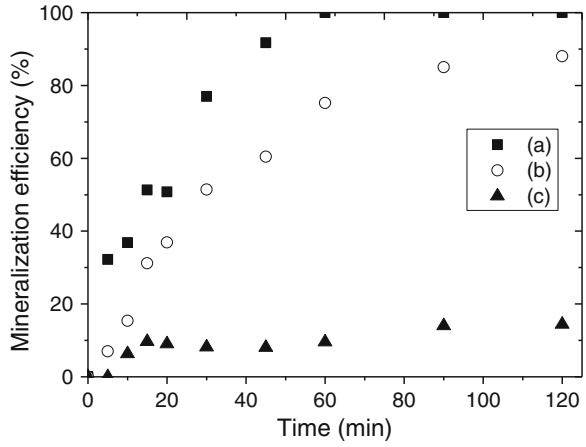

Fig. 1 Efficiency of mineralization: (*a*) wastewater without salts, (*b*) effluent with 100 ppm of each salt, and (*c*) effluent with 500 ppm of each salt

the absence of salts in 60 min of a reaction was complete (Fig. 1a). However, with 100 ppm (Fig. 1b) and 500 ppm (Fig. 1c) of each salt, at 120 min of reaction, this efficiency was reduced to 85 and 14 %, respectively.

This inhibitor effect may be attributed to the following factors (Laat et al. 2004): (1) complexation reactions between ferrous and ferric ions can alter the distribution of reactive species, (2) precipitation reactions lead to the decreasing of dissolved iron concentration, (3) formation of radicals and radical ions with less oxidation capacity ($Cl^{-\bullet}$, $Cl_2^{-\bullet}$, and $SO_4^{-\bullet}$) and hydroxyl radical scavenger, and (4) oxidation reaction involving these inorganic radicals (Eqs. 7 and 8).

$$^{\bullet}OH + A^{n-} \rightarrow A^{\bullet((n-1)-)} + {}^{-}OH \quad (7)$$

$$Fe^{2+} + A^{\bullet((n-1)-)} \rightarrow Fe^{3+} + A^{n-} \quad (8)$$

where Fe^{2+} represents all the iron species, A^{n-} the inorganic anions, and $A^{\cdot((n-1)-)}$ the radical anions.

3.2 Fractional Factorial Design

Figure 2 shows the mineralization kinetics to the experiments 0 to 15 according to the fractional factorial design presented in Table 3. Figure 2a shows mineralization kinetics to the experiments 0 (absence of salts) and 1, 2, 3, 5, and 9, where the total salt concentration was 790 ppm. In the curves 1, 2, 3, and 5, the sodium monophosphate concentration was at the inferior level (−1), whereas further variables alternated between the maximum and minimum conditions, according to the experimental design presented in Table 3. Curve 9 presents mineralization efficiency that is lower than the other conditions, where sodium monophosphate concentration is at level +1. In comparing curve 9 to the others, it is clear that the inhibitor effect was caused by monophosphate on phenol mineralization when leaving level −1 to +1. Experimental conditions from the runs 4, 6, 7, 8, and 10 to 15 (Table 3) correspond to salt total concentration of 1,370 ppm. As can be seen in Fig. 2b, the runs 4, 6, 7, and 8 (x_4 in level −1) present better mineralization efficiency when compared to the efficiency of the runs 10 to 15 (x_4 in level +1). This indicates that the increase of $H_2PO_4^-$ ions concentration in the reaction medium significantly affects the phenol mineralization.

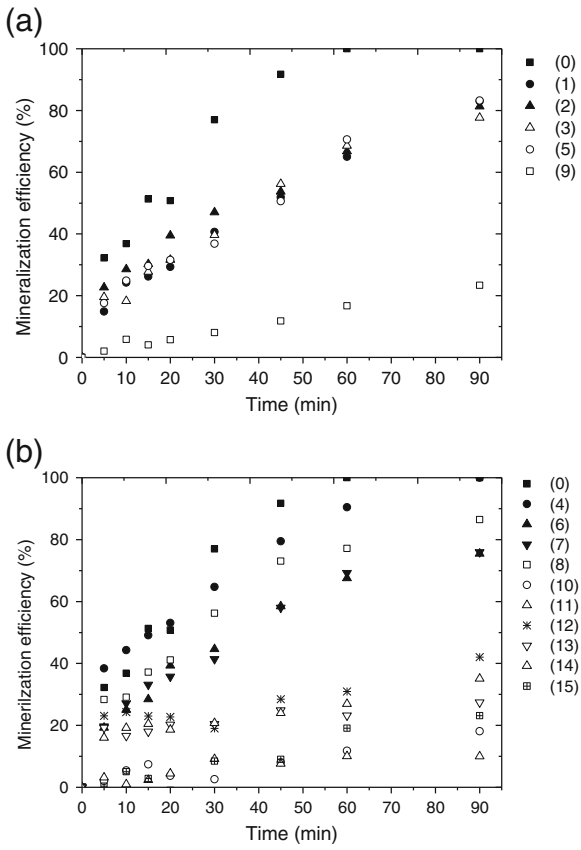

Fig. 2 Efficiency of phenol mineralization according the coded values of the experimental design for the variables x_1, x_2, x_3, x_4, and x_5. (**a**) Curve 0 (without salts), curve 1 (−1, −1, −1, −1, +1), curve 2 (+1, −1, −1, −1, −1), curve 3 (−1, +1, −1, −1, −1), curve 5 (−1, −1, +1, −1, −1), curve 9 (−1, −1, −1, +1, −1); (**b**) curve 4 (+1, +1, −1, −1, +1), curve 6 (+1, −1, +1, −1, +1), curve 7 (−1, +1, +1, −1, +1), curve 8 (+1, +1, +1, −1, −1), curve 10 (+1, −1, −1, +1, +1), curve 11 (−1, +1, −1, +1, +1), curve 12 (+1, +1, −1, +1, −1), curve 13 (−1, −1, +1, +1, +1), curve 14 (+1, −1, +1, +1, −1), and curve 15 (−1, +1, +1, +1, −1)

Table 3 shows a comparison between the observed and predicted values of phenol mineralization at 90 min of reaction. The coefficients were determined by correlating the experimental data with the response function (y_i) using Statistica 7.0 software. The response function is presented in terms of the efficiency of phenol mineralization (y), with R^2=0.95. The model was described considering the interactions between two variables (Eq. 9).

$$\begin{aligned} y = {} & 54.89 + 1.91x_1 + 1.17x_2 + 0.11x_3 - 27.01x_4 \\ & - 4.46x_5 + 4.41x_1x_2 - 2.38x_1x_3 - 1.32x_1x_4 \\ & + 0.71x_1x_5 - 0.19x_2x_3 - 1.27x_2x_4 - 0.45x_2x_5 \\ & + 2.41x_3x_4 - 1.16x_3x_5 - 4.87x_4x_5 \end{aligned} \quad (9)$$

Table 3 Coded levels for the fractional factorial design used for the response surface methodology (RSM) analysis of the inorganic ions in phenol mineralization

Run	x_1	x_2	x_3	x_4	x_5	Observed mineralization[a] (%)	Predict mineralization[a] (%)
0	–	–	–	–	–	100	–
1	−1	−1	−1	−1	1	83.0	81.7
2	1	−1	−1	−1	−1	81.3	80.0
3	−1	1	−1	−1	−1	77.7	76.4
4	1	1	−1	−1	1	100.0	98.7
5	−1	−1	1	−1	−1	83.2	81.9
6	1	−1	1	−1	1	75.5	74.2
7	−1	1	1	−1	1	76.0	74.7
8	1	1	1	−1	−1	88.9	87.6
9	−1	−1	−1	1	−1	36.4	35.1
10	1	−1	−1	1	1	18.1	16.8
11	−1	1	−1	1	1	10.0	8.7
12	1	1	−1	1	−1	42.0	40.8
13	−1	−1	1	1	1	27.4	26.1
14	1	−1	1	1	−1	35.1	33.8
15	−1	1	1	1	−1	40.4	39.2
16	1	1	1	1	1	23.8	22.5
17	0	0	0	0	0	46.2	54.9
18	0	0	0	0	0	61.4	54.9
19	0	0	0	0	0	41.2	54.9
20	0	0	0	0	0	67.4	54.9
21	0	0	0	0	0	42.9	54.9
22	0	0	0	0	0	47.9	54.9

[a] Mineralization efficiency at 90 min

According to Eq. (9), the negative coefficients represent variables that negatively affect the mineralization efficiency, whereas the positive ones are favorable to this process. In Pareto's graphic (Fig. 3), the values of the standard effects are shown in horizontal bars. Those factors that exceed the dotted line represent the variables with a remarkable effect on the response variable, at a 95 % confidence level. From Fig. 3, it can be observed that only the variable x_4 is statistically significant. According to diagrams of phosphate speciation, the $H_2PO_4^-$ ion predominates in pH=3 (Butler and Cogley 1998). This ion will react with dissolved iron, thereby leading to the formation of complexes that reduce the degradation rate (Eqs. 10 and 11).

$$Fe^{2+} + H_2PO_4^- \rightarrow FeH_2SO_4^{1+} \quad (10)$$

$$Fe^{3+} + H_2PO_4^- \rightarrow FeH_2SO_4^{2+} \quad (11)$$

To find out the composition of the salt mixtures that led to less mineralization efficiency, i.e., where there is the most inhibitor effect, contour curves were plotted with all the combinations among the independent variables (Fig. 4). Figure 4d–f, j shows that the phosphate concentration increasing from the inferior (−1) to the superior (+1) level leads to a remarkable reduction of efficiency. On the other hand, the effects of the concentration of the other salts were not remarkable for the response variable, as it is shown in Fig. 4a–c, g–i. The most highlighted phosphate effect can be attributed to the precipitation reactions between iron and phosphate ions.

The lack of statistical significance of the other anions NO_3^-, Cl^-, SO_4^{2-}, and CO_3^{2-} upon the response variable represents that, in the concentration range studied, these variables do not affect phenol mineralization. Anions NO_3^- and CO_3^{2} do not react with iron ions in order to form complexes. Its main inhibitor effect is attributed to the hydroxyl radical scavenging (Eqs. 12 and 13) (Riga et al. 2007; Devi et al. 2011). Thus, the reaction between Fe(III) and hydrogen peroxide is not suppressed.

$$NO_3^- + {}^{\bullet}OH \rightarrow NO_3^{\bullet} + {}^{-}OH \quad (12)$$

$$CO_3^{2-} + {}^{\bullet}OH \rightarrow CO_3^{\bullet -} + {}^{-}OH \quad (13)$$

The literature reports that both chloride and sulfate ions lead to the reduction of organic dye mineralization (Riga et al. 2007; Devi et al. 2011), whereas chloride ions can reduce the phenol mineralization (Maciel et al. 2004) in an aqueous solution by photo-Fenton. Based on this, a new experimental design was performed with chloride and sulfate as independent variables, according to the levels presented in Table 2.

The standard deviation of the responses at the central point (runs 17 to 22 in Table 3) was 10.3 %. This value may be attributed to the experimental procedure once it was necessary and the dilution of the samples for the TOC measurements due to the high content of salts. In this set of experiments, the system comprised five salts increasing the mixture operations, thereby contributing to the increment of the experimental error. This is also coherent with the studied system with two salts presenting a lower standard deviation (1.7 %) of the central points (see runs 9 to 13 of Table 5). Analysis of variance (ANOVA) indicates a fractional factorial model with 95 % of confidence (Table 4). Correlation between the experimental data and calculated values by the model

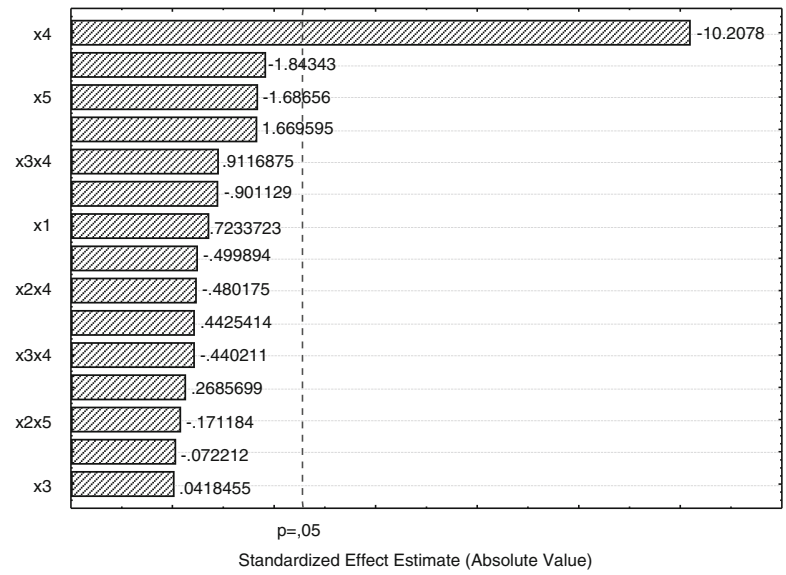

Fig. 3 Pareto graph for phenol mineralization by photo-Fenton as a function of sodium chloride (x_1), sodium sulfate (x_2), sodium carbonate (x_3), sodium monophosphate (x_4), and sodium nitrate (x_5) concentrations

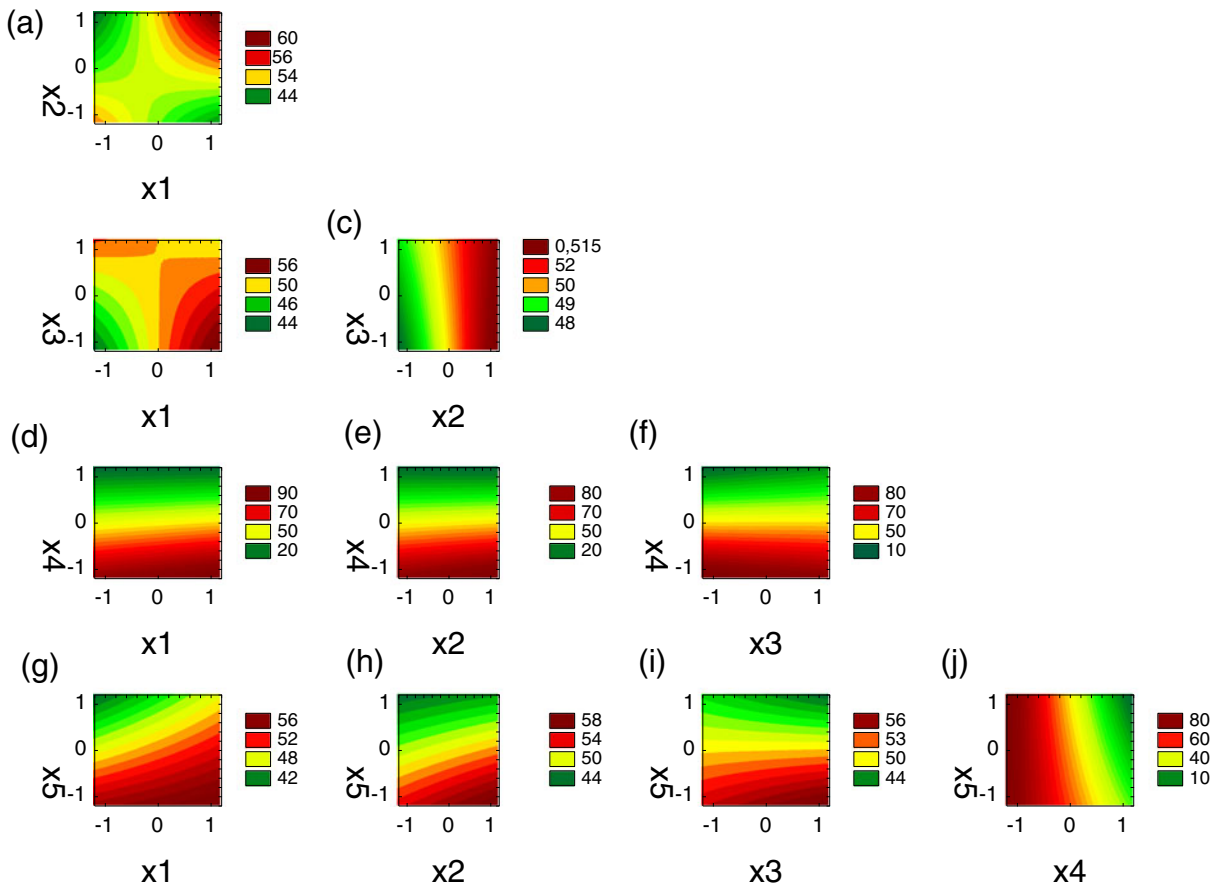

Fig. 4 Contour plots of phenol mineralization as a function of the coded value: sulfate versus chloride (**a**), carbonate versus chloride (**b**), carbonate versus sulfate (**c**), monophosphate versus chloride (**d**), monophosphate versus sulfate (**e**), monophosphate versus carbonate (**f**), nitrate versus chloride (**g**), nitrate versus sulfate (**h**), nitrate versus carbonate (**i**) versus nitrate, and monophosphate (**j**)

Table 4 Analysis of variance (ANOVA) for phenol mineralization

Design	Source	Sum of squares	Degrees of freedom	Mean square	*F* value	$F_{tabulated}$
Fractional factorial	Model	13,038.02	15	869	7.94	3.94
	Residual	657.13	6	110	–	–
	Lack of fit	96.95	1	97	0.87	6.61
	Pure error	560.17	5	112	–	–
	Total	13,695.14	21			
	R^2=0.9520					
	R^2_{adj}=0.8321					
Central composite rotatable	Model	133.08	5	26.62	11.03	3.97
	Residual	10.30	7	1.47	–	–
	Lack of fit	6.37	3	2.12	0.68	6.59
	Pure error	4.42	4	1.11	–	–
	Total	143.38	12			
	R^2=0.8798					
	R^2_{adj}=0.7939					

was satisfactory (R^2=0.9520). Test *F* (Fisher distribution) was applied to the obtained model, to verify that the model is predictive for the concentration range studied.

3.3 Central Composite Rotatable Design

The Central Composite Rotatable Design (CCRD) was performed according to the levels presented in Table 2. Table 5 shows the codified values and mineralization efficiencies that were observed for each condition tested at 60 min. Mineralization efficiencies ranged from 81 to 94 %, when the highest and lowest sodium chlorite concentrations were used, respectively. The mineralization data that were obtained by design were correlated in order to obtain the coefficients of response function for the dependent variables (Eq. 14).

$$y = 90.07 - 3.81x_1 - 1.14x_1^2 - 0.23x_2 - 0.68x_2^2 + 1.64x_1x_2 \quad (14)$$

From Pareto's diagram, as shown in Fig. 5, it is observed that only the sodium chlorite concentration was statistically significant, and the effect of this variable is negative upon mineralization efficiency. Sulfate and chloride anions act in the inhibition of the reaction through the formation of complexes with iron ions and in the hydroxyl radical scavenging (Eqs. 15–24). The radicals formed $Cl^{\bullet}$(E^o=2.41 V), $SO_4^{\bullet -}$(E^o=2.43 V) and $HO_2^{\bullet}$(E^o=1.80 V) are also an oxidant species, but they reduce the degradation rate because of their lower oxidation potential in relation to that of hydroxyl radical (Siedlecka et al. 2007).

$$SO_4^{2-} + HO^{\bullet} \rightarrow SO_4^{-\bullet} + HO^- \quad (15)$$

$$Fe^{2+} + SO_4^{2-} \leftrightarrow Fe\,SO_4 \quad (16)$$

Table 5 Coded levels for central composite rotatable design used for the RSM analysis of the inorganic ions in phenol mineralization

Run	x_1	x_2	Observed mineralization[a] (%)	Predict mineralization[a] (%)
0	–	–	100	–
1	−1.41	0	93.6	93.2
2	1.41	0	81.0	82.4
3	−1	1	89.8	90.2
4	−1	−1	94.1	93.9
5	1	−1	84.5	83.0
6	1	1	86.8	85.8
7	0	−1.41	88.1	89.0
8	0	1.41	88.2	88.4
9	0	0	89.4	90.1
10	0	0	88.5	90.1
11	0	0	88.6	90.1
12	0	0	91.9	90.1
13	0	0	92.0	90.1

[a] Mineralization efficiency at 60 min

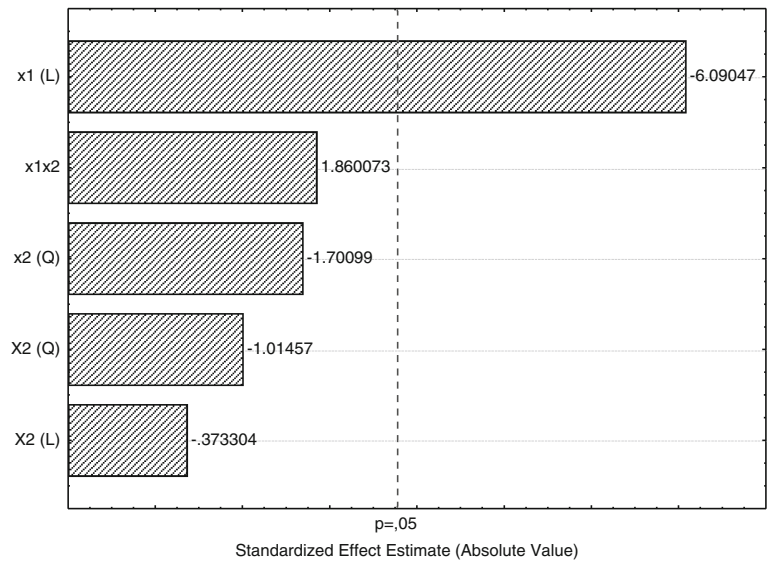

Fig. 5 Pareto's graph for phenol mineralization by photo-Fenton as a function of sodium chloride (x_1) and sodium sulfate (x_2) concentrations

$$Fe^{3+} + SO_4^{2-} \leftrightarrow Fe\,SO_4^{+} \quad (17)$$

$$SO_4^{2-} + {}^{\bullet}OH \rightarrow SO_4^{\bullet -} + {}^{-}OH \quad (18)$$

$$SO_4^{\bullet -} + H_2O_2 \rightarrow SO_4^{2-} + HO_2^{-\bullet} + H^{+} \quad (19)$$

$$Cl^{-} + {}^{\bullet}OH + H^{+} \rightarrow Cl^{\bullet} + H_2O \quad (20)$$

$$Cl^{\bullet} + H_2O_2 \rightarrow HO_2^{\bullet} + Cl^{-} + H^{+} \quad (21)$$

$$Cl^{\bullet} + HO^{\bullet} \rightarrow [ClOH]^{-\bullet} \quad (22)$$

$$Fe^{2+} + Cl^{-} \leftrightarrow FeCl^{+} \quad (23)$$

$$Fe^{3+} + Cl^{-} \leftrightarrow FeCl^{2+} \quad (24)$$

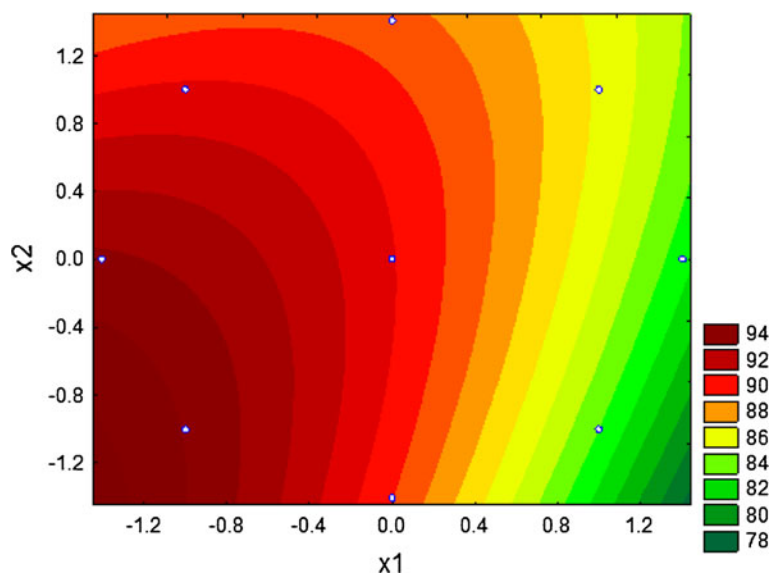

Fig. 6 Contour plots of phenol mineralization efficiency as a function of the coded values of the sodium chloride (x_1) and sodium sulfate (x_2) concentrations

The contour curve in Fig. 6 shows the chloride increase, from the inferior level (−1.41) to the superior (+1.41), which leads to a considerable decrease in efficiency. On the other hand, the concentration effect of sulfate is lower. The results of the ANOVA are presented in Table 4. The correlation between the experimental data and calculated values by the CCRD model was satisfactory (R^2=0.8798). Applying the Fisher distribution (F test), it was possible to observe that the model was significative and predictive. Thus, this model can be used to estimate mineralization efficiency in other experimental conditions of the domain studied in this work.

4 Conclusions

The experimental design results pointed out that phenol mineralization by photo-Fenton can be strongly affected by the presence of inorganic salts. Phenol mineralization efficiency ranged from 10 to 100 %, and this was quantified as a function of the concentration and type of the inorganic anions for the different sodium salts studied. The mineralization inhibition order was found to be: $H_2PO_4^- \gg Cl^- > SO_4^{2-} > NO_3^- \approx CO_3^{2}$. Among the evaluated salts, sodium monophosphate and sodium chloride presented the highest inhibition in the phenol mineralization. The ANOVA revealed: (1) good adjustment between the observed and predicted values (R^2= 0.95 and R^2=0.88, for fractional factorial design outlining and CCRD, respectively) and (2) according to Fisher distribution, the model obtained was considered significative and predictive.

Acknowledgments The Brazilian financial support that was provided by ANP (Agência Nacional do Petróleo, Gás Natural e Biocombustíveis), Petrobrás S.A., CAPES (Coordenação de Aperfeiçoamento de Pessoal de Nível Superior), CNPq (Conselho Nacional de Desenvolvimento Científico e Tecnológico), and INCT of Environmental Studies (Institutos Nacionais de Ciência e Tecnologia de Estudos do Meio Ambiente) is gratefully acknowledged.

References

Babuponnusami, A., & Muthukumar, K. (2011). Degradation of phenol in aqueous solution by Fenton, sono-Fenton and sono-photo-Fenton methods. *Clean - Soil Air Water, 39*, 142–147.

Bacardit, J., Stötzner, J., Chamarro, E., & Esplugas, S. (2007). Effect of salinity on the photo-Fenton process. *Industrial and Engineering Chemistry Research, 46*, 7615–7619.

Box, G. E. P., Hunter, J. S., & Hunter, W. G. (2005). *Statistics for experimenters: design, innovation, and discovery* (2ªth ed.). New Jersey: Wiley.

Butler, J. N., & Cogley, D. R. (1998). *Ionic equilibrium: solubility and pH calculations*. Canada: Wiley.

Devi, L. G., Kumar, S. G., Raju, K. S. A., & Rajashekhar, K. E. (2010). Photo-Fenton and photo-Fenton-like processes for the degradation of methyl orange in aqueous medium: influence of oxidation states of iron. *Chemical Papers, 64*, 378–385.

Devi, L. G., Raju, K. S. A., Kumar, S. G., & Rajashekhar, K. E. (2011). Photo-degradation of di azo dye Bismarck Brown by advanced photo-Fenton process: influence of inorganic anions and evaluation of recycling efficiency of iron powder. *Journal of the Taiwan Institute of Chemical Engineers, 42*, 341–349.

Gernjak, W., Krutzler, T., Glaser, A., Malato, S., Caceres, J., Bauer, R., et al. (2003). Photo-Fenton treatment of water containing natural phenolic pollutants. *Chemosphere, 50*, 71–78.

Huang, Y.-H., Huang, Y.-J., Tsai, H.-C., & Chen, H.-T. (2010). Degradation of phenol using low concentration of ferric ions by the photo-Fenton process. *Journal of the Taiwan Institute of Chemical Engineers, 41*, 699–704.

Kavitha, V., & Palanivelu, K. (2004). The role of ferrous ion in Fenton and photo-Fenton processes for the degradation of phenol. *Chemosphere, 55*, 1235–1243.

Krutzler, T., & Bauer, R. (1999). Optimization of a photo-Fenton prototype reactor. *Chemosphere, 38*, 2517–2532.

Laat, J., Le, G. T., & Legube, B. (2004). A comparative study of the effects of chloride, sulfate and nitrate ions on the rates of decomposition of H_2O_2 and organic compounds by Fe(II)/H_2O_2 and Fe(III)/ H_2O_2. *Chemosphere, 55*, 715–723.

Machulek, A., Jr., Moraes, J. E. F., Vautier-Giongo, C., Silverio, C. A., Friedrich, L. C., Nascimento, C. A. O., et al. (2007). Abatement of the inhibitory effect of chloride anions on the photo-Fenton process. *Environmental Science and Technology, 41*, 8459–8463.

Maciel, R., Sant'anna, G. L., Jr., & Dezotti, M. (2004). Phenol removal from high salinity effluents using Fenton's reagent and photo-Fenton reaction. *Chemosphere, 57*, 711–719.

Masomboon, N., Chen, C.-W., Anotai, J., & Lu, M.-C. (2010). A statistical experimental design to determine o-toluidine degradation by the photo-Fenton process. *Chemical Engineering Journal, 159*, 116–122.

Moraes, J. E. F., Quina, F. H., Nascimento, C. A. O., Silva, D. N., & Chiavone-Filho, O. (2004). Treatment of saline wastewater contaminated with hydrocarbons by the photo-Fenton process. *Environmental Science and Technology, 38*, 1183–1187.

Navarro, R. R., Ichikawa, H., & Tatsumi, K. (2010). Ferrite formation from photo-Fenton treated wastewater. *Chemosphere, 80*, 404–409.

Reis, M. T. A., Freitas, O. M. F., Agarwal, S., Ferreira, L. M., Ismael, M. R. C., Machado, R., et al. (2011). Removal of phenols from aqueous solutions by emulsion liquid membranes. *Journal of Hazardous Materials, 192*, 986–994.

Riga, A., Soutsas, K., Ntampegliotis, K., Karayannis, V., & Papapolymerou, G. (2007). Effect of system parameters and

of inorganic salts on the decolorization and degradation of Procion H-exl dyes. Comparison of H_2O_2/UV, Fenton, UV/Fenton, TiO_2/UV and TiO_2/UV/H_2O_2 processes. *Desalination, 211*, 72–86.

Rodrigues, L. A., Silva, M. L. C. P., Alvarez-Mendes, M. O., Coutinho, A. R., & Thima, G. P. (2011). Phenol removal from aqueous solution by activated carbon produced from avocado kernel seeds. *Chemical Engineering Journal, 74*, 49–57.

Saitoh, T., Asano, K., & Hiraide, M. (2011). Removal of phenols in water using chitosan-conjugated thermo-responsive polymers. *Journal of Hazardous Materials, 185*, 1369–1373.

Siedlecka, E. M., Wieckowska, A., & Stepnowski, P. (2007). Influence of inorganic ions on MTBE degradation by Fenton's reagent. *Journal of Hazardous Materials, 147*, 497–502.

Silva, S. S., Chiavone-Filho, O., Neto, E. L. B., & Nascimento, C. A. O. (2012). Integration of processes induced air flotation and photo-Fenton for treatment of residual waters contaminated with xylene. *Journal of Hazardous Materials, 199–200*, 151–157.

Teófilo, R. F., & Ferreira, M. M. C. (2006). Quimiometria II: Planilhas eletrônicas para cálculos de planejamentos experimentais, um tutorial. *Quimica Nova, 29*, 338–350.

Trinh, T. K., & Kang, L. S. (2011). Response surface methodological approach to optimize the coagulation–flocculation process in drinking water treatment. *Chemical Engineering Research and Design, 89*, 1126–1135.